

# Unprecedented Robust Antiferromagnetism in Fluorinated Hexagonal Perovskites

Mihai Sturza,<sup>†</sup> Houria Kabbour,<sup>†</sup> Sylvie Daviero-Minaud,<sup>†</sup> Dmitry Filimonov,<sup>‡</sup> Konstantin Pokholok,<sup>‡</sup> Nicolas Tiercelin,<sup>§</sup> Florence Porcher,<sup>||</sup> Laurent Aldon,<sup>⊥</sup> and Olivier Mentre<sup>\*,†</sup>

<sup>†</sup>Université Lille Nord de France, UCCS, CNRS UMR 8181, ENSCL-USTL, Villeneuve d'Ascq, France

<sup>‡</sup>Department of Chemistry, Moscow State University, 119991 Moscow, Russia

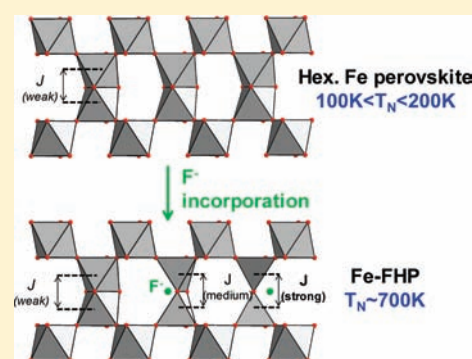
<sup>§</sup>International Associated Laboratory LEMAC: IEMN, UMR CNRS 8520, PRES Lille Nord de France, EC Lille, Villeneuve d'Ascq, France

<sup>||</sup>Laboratoire Léon Brillouin, CEA Saclay, 91191 Gif-sur-Yvette Cedex, France

<sup>⊥</sup>Université Montpellier 2, CNRS, Inst. Ch. Gerhardt, UMR 5253, France

 Supporting Information

**ABSTRACT:** The diversification of antiferromagnetic (AFM) oxides with high Néel temperature is of fundamental as well as technical interest if one considers the need for robust AFM in the field of spin-tronics (exchange bias, multiferroics, etc.). Within the broad series of so-called hexagonal perovskites (HP), the existence of face-sharing octahedral units drastically lowers the strength of magnetic exchanges as compared to corner-sharing octahedral edifices. Here, we show that the partial introduction of  $F^-$  in several Fe-based HP types leads to a drastic increase of the AFM ordering close to the highest values reported in iron oxides ( $T_N \approx 700$  K). Our experimental results are supported by ab initio calculations. The  $T_N$  increase is explained by the structural effect of the aliovalent  $F^-$  for  $O^{2-}$  substitution occurring in preferred anionic positions: it leads to local changes of the Fe–O–Fe connectivity and to chemical reduction into predominant  $Fe^{3+}$ , both responsible for drastic magnetic changes.



## INTRODUCTION

Even if antiferromagnetic (AFM) ordering is the most common case in nature, up to very recently, only little interest was given to AFM materials for technological applications. The situation has changed since the practical uses of giant- and tunnelling-magnetoresistant materials in the field of microelectronics and spintronics.<sup>1–3</sup> Here, strong pinning of soft ferromagnetic moments at the bilayered AFM/FM interface by exchange-bias is exploited.<sup>4,5</sup> The quest for performant devices has triggered an intense search for new antiferromagnets; particularly high performances require robust AFM materials, that is, high thermal stability of the AFM ordering.<sup>6</sup> The most technologically significant exchange bias AFM oxides are the rocksalt-structure such as NiO ( $T_N = 523$  K) or CoO ( $T_N = 293$  K) and their alloys.<sup>7,8</sup> However, the diversification of new advanced systems involves the research for similar properties in new types of coherent multilayered atomic interfaces. Within the prospection for oxides with high temperature magnetic ordering, iron appears as the privileged transition metal with the strongest spin value in high-spin  $Fe^{3+}$  ( $S = 5/2$ ). Recently, high  $T_N$  AFM Fe-based compounds have known another regain of interest with the emergence of multiferroic compounds in which the perovskite  $BiFeO_3$  ( $T_N = 643$  K,  $T_C = 1103$  K) is the most representative example.<sup>9</sup> Another example concerns the

bidimensional  $SrFeO_2$ , which results from the extreme topotactic reduction of  $SrFeO_{3-\delta}$ .<sup>10</sup> In this compound, the origin of the unusual high  $T_N = 473$  K is still under debate.<sup>11,12</sup> In the present work, we focus on an extended series of polymorphs originating from the perovskite, the Fe-based hexagonal perovskites. In these compounds, the existence of face-sharing octahedral units drastically lowers the 3D-expansion of magnetic interactions, resulting in weaker Fe–Fe magnetic interactions, as compared to corner-sharing assembly of standard 3D-perovskites. Here, we show that the partial substitution of  $O^{2-}$  for  $F^-$  in two hexagonal polytypes (15R and 6H)<sup>13</sup> strikingly enhances the Néel temperature up to unprecedented values in this family ( $T_N > 700$  K). It is explained on the basis of two concomitant effects of the  $F^-$  incorporation: (i) the  $F^-$  are preferentially incorporated in the hexagonal layers of the structures, leading to the modification of the Fe–Fe connectivity that reinforces the magnetic exchanges. (ii) The reduction of  $Fe^{4+}$  into  $Fe^{3+}$  species favors the strongest exchanges. We examine this aspect on the basis of powder neutron diffraction (PND), transport/magnetic measurements, Mössbauer spectroscopy, and density functional calculations.

Received: March 29, 2011

Published: June 07, 2011

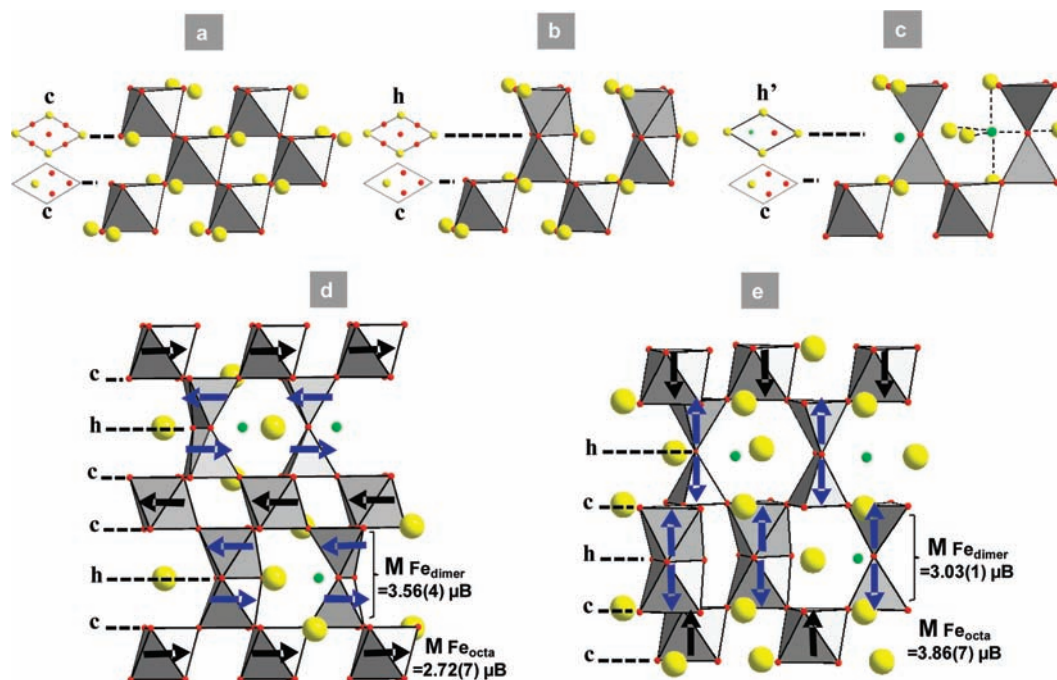


**Figure 1.** Incorporation of F<sup>-</sup> in hexagonal perovskites: (a) c-[BaO<sub>3</sub>] layers leading to corner-sharing octahedra. (b) h-[BaO<sub>3</sub>] leading to face-sharing octahedra. (c) h'-[BaOF] layers leading to corner-sharing tetrahedra. The ideal position for F<sup>-</sup> is at the center of a FBa<sub>5</sub> bipyramid. (d) Structure of the partially fluorinated 6H-polytype of sequence [chcchc] with mixture of several Fe configurations. (e) Structure of the 15R-FHP of sequence [cchch]<sub>3</sub>. The magnetic structure as refined from PND at room temperature is represented. For the 15R compounds, the moments were assumed similar in the two crystallographic sites Fe2 and Fe3 forming the dimers. For the 15R form, the thermal evolution of the moments is given in the Supporting Information.

## EXPERIMENTAL DETAILS

Black polycrystalline samples of 15R-BaFe<sub>x</sub>O<sub>3-δ</sub> (0.15 ≤ *x* ≤ 0.35) and 6H-Ba<sub>0.8</sub>Sr<sub>0.2</sub>Fe<sub>x</sub>O<sub>3-δ</sub> (0.15 ≤ *x* ≤ 0.25) have been obtained through solid-state reaction using stoichiometric mixtures of BaO<sub>2</sub> (Aldrich 95%), SrO<sub>2</sub> (Aldrich 95%), Fe<sub>2</sub>O<sub>3</sub> (Aldrich 99%), and BaF<sub>2</sub> (Aldrich 99%) as starting materials. The mixtures were ground in an agate mortar and placed in closed (but not sealed) gold tubes. The samples were subsequently heated 48 h at 900 °C for BaFe<sub>x</sub>O<sub>3-δ</sub> and 950 °C for Ba<sub>0.8</sub>Sr<sub>0.2</sub>Fe<sub>x</sub>O<sub>3-δ</sub> and then quenched to room temperature. After this stage, the compounds are denoted “as-prepared”, which corresponds to a partially reduced state. Only the “in-tube” reaction allows a stoichiometric incorporation of F<sup>-</sup> in HP (→FHP). Out of the concerned *x* range, samples are found polyphased.<sup>13</sup> Also, following the method described in ref 14 the 6H-oxide-BaFeO<sub>3-δ</sub> (δ = 0.15 according to our titration) was prepared under flowing oxygen, for comparison of magnetic properties with FHP. This compound transforms into a cubic-BaFeO<sub>3-δ</sub> above 900 °C in air. It has not been possible to stabilize a “reduced” 6H-oxide because the lowest Fe-oxidation state obtained after heating/cooling at 900 °C in air corresponds to δ = 0.3. Finally, attempts to reduce the 6H-oxide in dynamic vacuum at 800 °C led to a mixture of the monoclinic-BaFeO<sub>2.5</sub> and BaFe<sub>2</sub>O<sub>4</sub>.

XRD-powder patterns were collected on a Bruker D8 diffractometer, (Cu<sub>Kα</sub> radiation) eventually using a high temperature Anton-Paar HTK1200 system under various flowing atmosphere as indicated in the text.

PND-powder analysis was performed on three samples: the 15R-BaFe<sup>+3.04</sup>F<sub>0.2</sub>O<sub>2.42</sub>, BaFe<sup>+3.08</sup>F<sub>0.2</sub>O<sub>2.44</sub>, and Ba<sub>0.8</sub>Sr<sub>0.2</sub>Fe<sup>+3.16</sup>F<sub>0.2</sub>O<sub>2.48</sub> at the Laboratoire Léon-brillouin (LLB) Saclay, France on the 3T2 diffractometer (λ = 1.2254 Å). For the 15R compound, the magnetic structures from room-temperature to 1.8 K were refined from data collected with the G41 diffractometer (λ = 2.4226 Å). Powder-XRD and ND data were analyzed with the Rietveld method using the FULLPROF 2000 program.<sup>15</sup>

Thermogravimetric analysis (TGA) and differential thermal analysis (DTA) were carried out using a combined TG-DTA 92-1600 SETARAM analyzer. Successive heating/cooling cycles were performed using a rate of 5 °C/min.

The oxidation state of iron was determined by a red–ox titration method. The samples were dissolved in a H<sub>3</sub>PO<sub>4</sub>/H<sub>2</sub>SO<sub>4</sub> acidic medium with an excess of Mohr-salt. The formal Fe<sup>4+</sup> reacts with Fe<sup>2+</sup>, leading to Fe<sup>3+</sup> formation. The amount of remaining Fe<sup>2+</sup> ions is determined by back-titration with a 0.1 M KMnO<sub>4</sub> solution.

Magnetization cycles and magnetization versus temperature were applied using an ADE EV9 vibrating sample magnetometer (VSM). Samples were heated during the measurements via a heated gas flow (air and N<sub>2</sub>) in a thermally isolated tube.

Mössbauer <sup>57</sup>Fe spectroscopy was performed in a transmission mode using a constant acceleration Mössbauer spectrometer (MS1104, Rostov-na-Donu, Russia) with a <sup>57</sup>Co/Rh γ-ray sources equipped with a high temperature setup. Velocities were calibrated with standard α-Fe or sodium nitroprusside absorbers; isomer shifts were related to α-Fe. Spectra treatment was performed using custom software.

## COMPUTATIONAL METHODS

Density functional theory (DFT) calculations were performed using the Vienna ab initio simulation package.<sup>16</sup> The calculations were carried out within the generalized gradient approximation (GGA) for the electron exchange and correlation corrections using the Perdew–Wang<sup>17</sup> functional and the frozen core projected wave vector method.<sup>18</sup> The full geometry optimizations were carried out using a plane wave energy cutoff of 550 eV and 42 or 50 *k* points (depending on the structural model) in the irreducible Brillouin zone. All structural optimizations converged with residual Hellman–Feynman forces on the atoms smaller than 0.03 eV/Å. The geometry optimizations were performed using nonspin-polarized calculations so that no magnetic configuration

Table 1.  $^{57}\text{Fe}$  Mossbauer Hyperfine Parameters of 15R- and 6H-FHP<sup>a</sup>

| compound  | T, K | component | IS, mm/s $\pm$ 0.03 | $\Delta$ , mm/s $\pm$ 0.03 | $2\varepsilon$ , mm/s $\pm$ 0.05 | $H_{\text{hf}}$ , T $\pm$ 0.5 | $\Gamma$ , mm/s $\pm$ 0.05 | $I$ , (%) $\pm$ 2 | assign                                | PND (%)                                  |                     |
|---|------|-----------|---------------------|----------------------------|----------------------------------|-------------------------------|----------------------------|-------------------|---------------------------------------|--|---------------------|
| 15R-BaFeF <sub>0.2</sub> O <sub>~2.42</sub>                                 | 298  | A1        | 0.37                |                            | 0.1                              | 50.2                          | 0.3                        | 6                 | Fe <sup>3+</sup> <sub>Oh</sub>        | 20 Fe <sup>3+</sup> <sub>Oh</sub>        |                     |
|   |      | A2        | 0.37                |                            | 0                                | 49                            | 0.4                        | 10                |                                       |  |                     |
|   |      | A3        | 0.25                |                            | -0.5                             | 47                            | 0.34                       | 18                | Fe <sup>3+</sup> <sub>dim(V,VI)</sub> | 56 Fe <sup>3+</sup> <sub>dim(V,VI)</sub> |                     |
|   |      | A4        | 0.19                |                            | 0.1                              | 46                            | 0.5                        | 40                |                                       |  |                     |
|   |      | A5        | 0.21                |                            | -0.2                             | 43                            | 0.4                        | 13                | Fe <sup>3+</sup> <sub>dim(IV)</sub>   | 23 Fe <sup>3+</sup> <sub>dim(IV)</sub>   |                     |
|   |      | A6        | -0.09               |                            | 0                                | 23.5                          | 0.45                       | 12                | Fe <sup>4+</sup> <sub>Oh</sub>        |  |                     |
|   |      | A7        | -0.11               | 1.33                       |                                  |                               |                            | 0.75              | 3                                     | Fe <sup>+3.15</sup>                      | Fe <sup>+3.04</sup> |
| 15R-BaFeF <sub>0.2</sub> O <sub>~2.42</sub>                                 | 750  | B1        | 0.04                | 0.79                       |                                  |                               | 0.39                       | 26                | Fe <sup>3+</sup> <sub>Oh</sub>        |  |                     |
|   |      | B2        | -0.12               | 0.74                       |                                  |                               | 0.4                        | 46                | Fe <sup>3+</sup> <sub>dim(V)</sub>    |  |                     |
|   |      | B3        | -0.03               | 0.2                        |                                  |                               | 0.35                       | 28                | Fe <sup>3+</sup> <sub>dim(IV)</sub>   |  |                     |
| 6H-Ba <sub>0.8</sub> Sr <sub>0.2</sub> Fe <sub>0.2</sub> O <sub>~2.48</sub> | 298  | C1        | 0.38                |                            | 0                                | 49.5                          | 0.6                        | 18                | Fe <sup>3+</sup> <sub>Oh</sub>        | 33 Fe <sup>3+</sup> <sub>Oh</sub>        |                     |
|   |      | C2        | 0.17                |                            | 0.25                             | 48                            | 0.35                       | 11                | Fe <sup>3+</sup> <sub>dim(V,VI)</sub> | 43 Fe <sup>3+</sup> <sub>dim(V,VI)</sub> |                     |
|   |      | C3        | 0.2                 |                            | -0.06                            | 45                            | 0.51                       | 23                |                                       |  |                     |
|   |      | C4        | 0.19                |                            | -0.13                            | 42                            | 0.45                       | 9                 | Fe <sup>3+</sup> <sub>dim(IV)</sub>   | 22 Fe <sup>3+</sup> <sub>dim(IV)</sub>   |                     |
|   |      | C5        | 0.24                |                            | 0                                | 36                            | 0.8                        | 6                 | Fe <sup>3+</sup>                      |  |                     |
|   |      | C6        | 0.32                | 0.63                       |                                  |                               |                            | 0.47              | 15                                    |  |                     |
|   |      | C7        | -0.08               |                            | 0                                | 25                            | 1                          | 13                | Fe <sup>4+</sup> <sub>Oh</sub>        |  |                     |
|   |      | C8        | -0.08               | 0                          |                                  |                               |                            | 1.5               | 6                                     | Fe <sup>+3.19</sup>                      | Fe <sup>+3.16</sup> |
| 6H-Ba <sub>0.8</sub> Sr <sub>0.2</sub> Fe <sub>0.2</sub> O <sub>~2.48</sub> | 750  | D1        | 0.03                | 0.7                        |                                  |                               | 0.4                        | 33                | Fe <sup>3+</sup> <sub>Oh</sub>        |  |                     |
|   |      | D2        | -0.12               | 0.71                       |                                  |                               | 0.4                        | 31                | Fe <sup>3+</sup> <sub>dim(V)</sub>    |  |                     |
|   |      | D3        | -0.05               | 0.2                        |                                  |                               | 0.34                       | 22                | Fe <sup>3+</sup> <sub>dim(IV)</sub>   |  |                     |
|   |      | D4        | -0.05               |                            | 0.25                             | 32                            | 0.37                       | 13                | impurity                              |  |                     |

<sup>a</sup> IS, isomer shift relative to  $\alpha$ -Fe at ambient temperature;  $\Delta$ , quadrupole splitting;  $\varepsilon$ , apparent quadrupole shift;  $\Gamma$ , line-width;  $I$ , relative area.

is favored. The structural models 6H-BaFeO<sub>3</sub>, 6H-BaFeO<sub>2.66</sub>F<sub>0.33</sub>, and 6H-BaFeO<sub>2.33</sub>F<sub>0.33</sub> were built from the initial structure of 6H-BaFeO<sub>3</sub> and then fully relaxed as described above. For the total energies calculations, GGA plus on-site repulsion (GGA+U)<sup>19</sup> calculations were employed to account for the strong electron correlation associated with the 3d electrons on the Fe atoms. A plane wave energy cutoff of 400 eV, a total energy convergence threshold of 10<sup>-6</sup>, and 91 or 98 *k* points (depending on the structural model) in the irreducible Brillouin zone were used.

## RESULTS AND DISCUSSION

**Structural Disorder in FHP.** The ABO<sub>3</sub> hexagonal perovskites display various stacking sequences of closed-packed [AO<sub>3</sub>] layers that include both hexagonal (h) between face-sharing octahedral (BaMnO<sub>3</sub> type)<sup>20</sup> and cubic (c) layers between corner-sharing octahedral (LaMnO<sub>3</sub> type).<sup>21</sup> In this family, F<sup>-</sup> ideally incorporate anionic-deficient h-[BaFO] layers in which F<sup>-</sup> and O<sup>2-</sup> occupy distinct crystallographic positions, yielding B<sub>2</sub>O<sub>7</sub> pairs of corner-sharing tetrahedra and FBa<sub>5</sub> bipyramid, Figure 1a–c. We have recently prepared 6H (with the [chcchc] stacking sequence, Figure 1d) and 15R (with the [cchc] stacking sequence, Figure 1e) (Ba,Sr)<sub>1</sub>Fe<sub>1</sub>O<sub>3-x</sub>F<sub>y</sub> fluorinated-hexagonal-perovskites (FHP).<sup>13</sup> In absence of fluorine, the 15R- form was only stabilized by a significant substitution of iron for a tetravalent metal (Ir<sup>4+</sup>, Mn<sup>4+</sup>),<sup>22,23</sup> while we obtained single-phase 15R-BaFeF<sub>x</sub>O<sub>3- $\delta$</sub>  for 0.15 < *x* < 0.35. The replacement of 20% Ba for Sr leads to 6H-Ba<sub>0.8</sub>Sr<sub>0.2</sub>FeF<sub>x</sub>O<sub>3- $\delta$</sub>  for 0.15 < *x* < 0.25. Here, also the

formation is favored by F<sup>-</sup> because the nonfluorinated specimen is prepared under oxygen pressure<sup>14</sup> in contrary to our syntheses (see Experimental Details). The prepared FHP corresponds to intermediate degrees of fluorination of the hexagonal layers, leading to disordered h-[BaOF<sub>1-x</sub>O<sub>3-y</sub>] layers at the basis of extended defect structures. Even if minor in terms of concentration, these defects are responsible for drastic magnetic changes. In fact, oxygen vacancies favor the displacement of part of the F<sup>-</sup> out of their ideal positions toward the metal positions. As previously verified, variously sized dimers then cohabit in the same blocks, Fe<sub>2</sub>O<sub>7</sub> tetrahedral and Fe<sub>2</sub>(O,F)<sub>9-x</sub> pyramidal/octahedral pairs; see Figure 1e.<sup>13</sup> Apart from this structural modification, the reducing effect of F<sup>-</sup> when introduced in anionic array is drastic, for example, from the ideal 6H-[chcchc]BaFe<sup>4+</sup>O<sub>3</sub> to 6H'-[ch'cch'c]BaFe<sup>+2.8</sup>F<sub>0.4</sub>O<sub>2.2</sub> after complete fluorination of h-[BaO<sub>3</sub>] layers into h'-[BaOF] layers. It is clear that the increased concentration of Fe<sup>3+</sup> cations should reinforce the magnetic interactions. Experimental evidence for the simultaneous presence of several Fe-coordinations is given by PND data for selected 15R and 6H compounds, Table 1.

Typically, in their as-prepared states, we refined ~30–35% of [Fe<sub>2</sub>O<sub>7</sub>] tetrahedral pairs versus 70–65% of [Fe<sub>2</sub>(O,F)<sub>9-x</sub>] pyramidal/octahedral pairs (see Supporting Information S1 data) assorted with a mean valence close to Fe<sup>3+</sup> in agreement with our redox titrations. By comparison, the particular role of iron is highlighted by previous results on the 5H-Ba<sub>5</sub>Co<sub>5</sub>XO<sub>13- $\delta$</sub>  and 12H-Ba<sub>6</sub>Co<sub>6</sub>XO<sub>16- $\delta$</sub>  (X = F<sup>-</sup>, Cl<sup>-</sup>) polytypes. In fact, in these compounds, halides also incorporate central hexagonal layers, but in an almost stoichiometric way, leading to [BaOX<sub>1- $\delta$</sub> ] layers

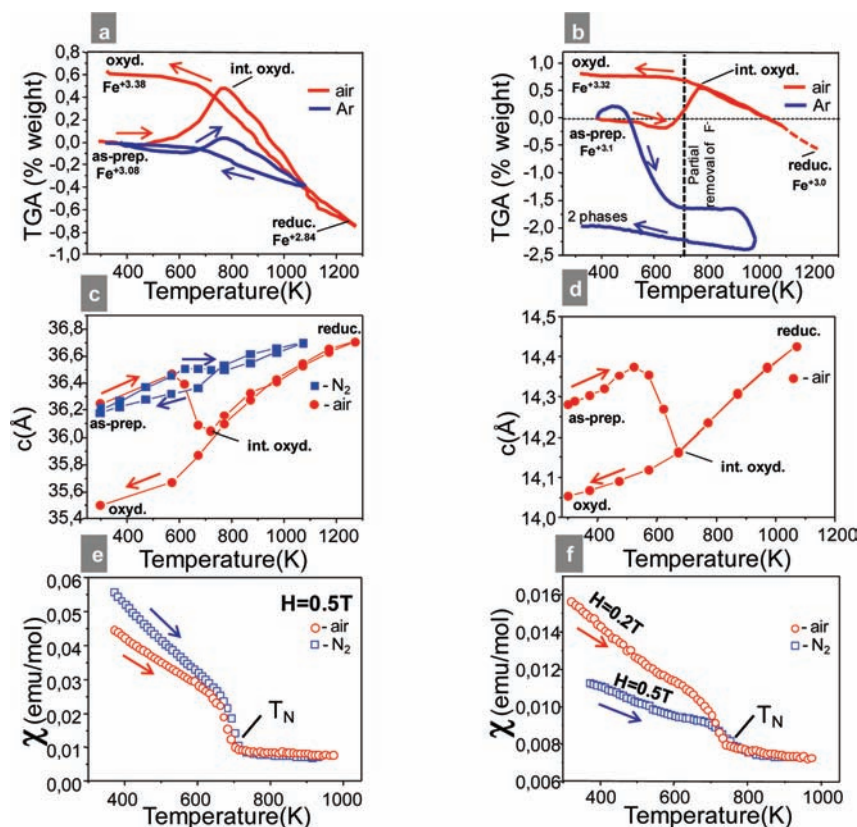


**Figure 2.** Thermal gravimetric analysis, evolution of the *c*-lattice parameter, and thermal susceptibility under various atmosphere for (a,c,e) 15R-BaFeF<sub>0.2</sub>O<sub>~2.44</sub> and (b,d,f) 6H-Ba<sub>0.8</sub>Sr<sub>0.2</sub>Fe<sub>0.2</sub>O<sub>~2.45</sub>. The mean valence state for iron was deduced from PND/redox titration at room temperature and assumed at highest temperature from TGA curves.

bordered by Co<sub>2</sub>O<sub>7</sub> tetrahedral-pairs only,<sup>24–27</sup> which are stable upon thermal treatments.<sup>28–30</sup>

**Thermal Stability of FHP.** Preliminary to the investigation of high-temperature magnetism the basis of this work, it is necessary to mention the particular thermal behavior of as-prepared FHP. Contrary to the metastable fluorinated-cubic-perovskites,<sup>31</sup> these iron-FHPs show a good structural stability above 1000 °C because single-phased XRD patterns persist on several heating/cooling cycles. Also, elemental analyses after long thermal treatments at 900 °C show no significant fluorine removal for the 15R-BaFeF<sub>y</sub>O<sub>3–x</sub> compounds, while a sensitive deviation of ~50% of the introduced fluoride content has been quantified in the 6H-Ba<sub>0.8</sub>Sr<sub>0.2</sub>FeF<sub>y</sub>O<sub>3–x</sub> compound. In contrast to the cubic AF<sub>2</sub>OF (A = Ba,Sr), which decomposes at 750 °C into AF<sub>2</sub> salts,<sup>31</sup> the striking stability of Fe-FHP is made possible by the reversible reorganization, upon heating/cooling, of the anionic array (O<sup>2–</sup>, F<sup>–</sup>, and vacancies) within the disorganized h-layers.<sup>13</sup> Next, under flowing air, both the 6H and the 15R as-prepared compounds undergo a reversible partial oxidation between 600 and 800 K but remain single-phased. The TGA and thermal dependence of the *c*-parameters are shown in Figure 2a–d. This behavior is accompanied by a significant increase of the concentration of octahedral dimers at the tetrahedral expense.<sup>13</sup> This effect is limited under neutral atmosphere as shown in Figure 2a,c for the 15R polytype. The 6H-form is more sensitive to redox variations, and the TGA under flowing Ar shows an irreversible partial reduction, which finally leads to a mixture of two 6H compounds. However, we observed by Mössbauer spectroscopy that this degradation is not efficient in static Ar, which enables a probing

of as-prepared state at high temperature. The particular relationship between the presence of F<sup>–</sup> and the creation of tetrahedra in the hexagonal-interleave has been discussed above, but is clearly depicted in Figure 3. On cooling from high to room temperature, we show the evolutions of the *c*-lattice parameter, and of the different Fe–Fe separations *d*<sub>1</sub> (across a h-layer) and *d*<sub>2</sub> (across a c-layer) projected along the *c*-axis for both the FHP 6H-Ba<sub>0.8</sub>Sr<sub>0.2</sub>FeF<sub>0.2</sub>O<sub>3–δ</sub> (*δ*: 0.6<sub>1000°C</sub> → 0.44<sub>RT</sub>) and the oxide 6H (*δ*: 0.47<sub>900°C</sub> → 0.3<sub>RT</sub>). Clearly, the much greatest expansion-parameter for the oxofluoride is achieved by the “breathing” effect of *d*<sub>1</sub> ( $\Delta d = 0.28$  Å) due to the octahedral-pairs into tetrahedral-pairs transformation of tetrahedral pairs in the hexagonal interleave.<sup>13</sup> In the corresponding oxide, the amplitude of the *d*<sub>1</sub> expansion ( $\Delta d = 0.16$  Å) is much lower, especially taking into account that the high-temperature distance merely coincides with those at room temperature for the oxofluoride. This feature plays in favor of the conservation of the octahedral pairs in this latter, even in its partially reduced high-temperature form. We will see later the fundamental importance of tetrahedral-pairs on the magnetic properties. Once more, one should recall that our attempts to reduce more the 6H-oxide failed; see Experimental Details.

**Magnetic Properties.** Even at room temperature, the PND data show heavy magnetic contributions, which correspond to the 3D-AFM ordering. The refinement of the two magnetic structures gives similar site-to-site antiparallel topologies, with respect to the propagation vector  $k = (0,0,0)$  in the 6H form (identical magnetic and structural unit cell) and  $k = (0,0,1/2)$  in the 15R form (doubled-*c* magnetic unit cell). We refined from

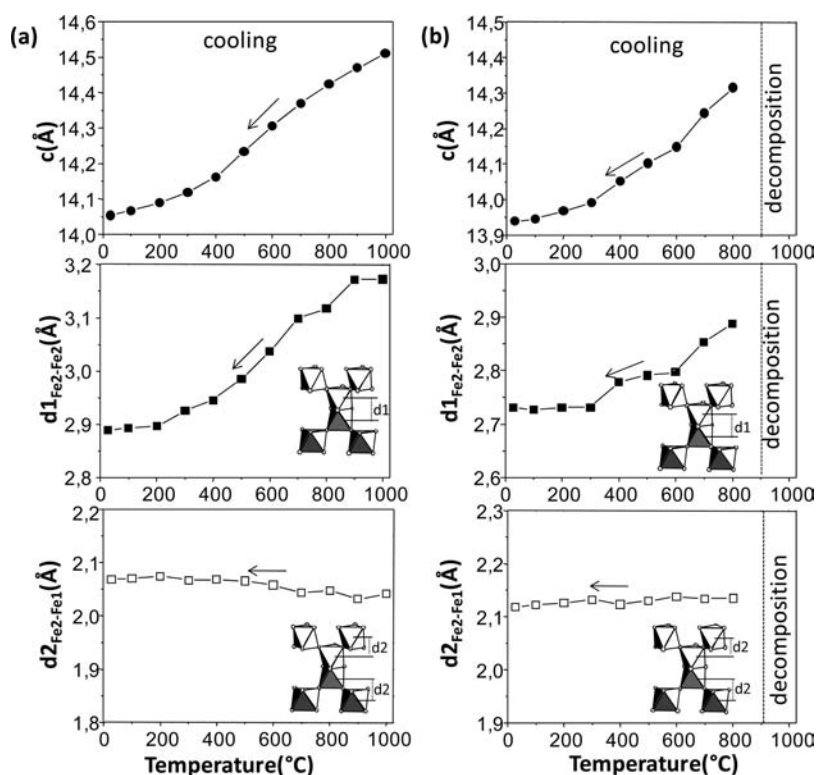
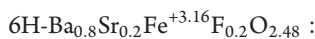
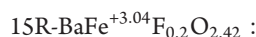


**Figure 3.** Thermal evolution of the  $c$ -lattice parameter and the intermetallic separations projected on the  $c$ -axis ( $d_1$ , interhexagonal slab Fe2–Fe2;  $d_2$ , cubic to hexagonal) upon cooling for (a)  $6\text{H-Ba}_{0.8}\text{Sr}_{0.2}\text{Fe}^{+3.16}\text{F}_{0.2}\text{O}_{2.48}$  and (b)  $6\text{H-BaFe}^{+3.7}\text{O}_{2.85}$ .

data collected at room temperature ( $\lambda = 1.22 \text{ \AA}$ , 3T2, LLB, Saclay, France):



$$\begin{aligned} M(\text{Fe}_{\text{octa}}) &= 2.72(7)\mu_{\text{B}} \text{ and} \\ M(\text{Fe}_{\text{dimer}}) &= 3.56(4)\mu_{\text{B}} \end{aligned}$$



$$\begin{aligned} M(\text{Fe}_{\text{octa}}) &= 3.86(7)\mu_{\text{B}} \text{ and} \\ M(\text{Fe}_{\text{dimer}}) &= 3.03(1)\mu_{\text{B}} \end{aligned}$$

The magneto-crystalline anisotropy is different for both compounds because moments lie in the  $(a,b)$  plane in the 6H-form and are aligned to the  $c$ -axis in the 15R-form, Figure 1d and e. The same site-to-site AFM ordering associated with similar disparity in terms of magnetocrystalline anisotropy was already reported for related compounds, for example, moments in the  $(a,b)$  planes in the 15R-SrMn<sub>0.9</sub>Fe<sub>0.1</sub>O<sub>3- $\delta$</sub>  ( $T_{\text{N}} = 220 \text{ K}$ ),<sup>23</sup> 15R-BaIr<sub>0.3</sub>Fe<sub>0.7</sub>O<sub>2.95</sub> ( $T_{\text{N}} = 200 \text{ K}$ ), and 6H-BaIr<sub>0.2</sub>Fe<sub>0.8</sub>O<sub>2.93</sub> ( $T_{\text{N}} = 220 \text{ K}$ )<sup>22</sup> and moments parallel to  $c$  in the 6H-BaFe<sub>0.66</sub>W<sub>0.33</sub>O<sub>3</sub> ( $200 \text{ K} < T_{\text{N}} < 300 \text{ K}$ ).<sup>32</sup> This behavior is hardly predictable because we have recently demonstrated the drastic effect of minor changes of the ratio of anionic vacancies on the orientation of the moments between the 5H and 12H forms BaCoF<sub>x</sub>O<sub>3- $y$</sub>  FHP.<sup>30</sup> One should recall that in these Co oxo-fluorides, the AFM ordering is different from what is observed in Fe-FHP but still involves strong AFM exchanges between two tetrahedra of the dimers.

The most striking magnetic features of FHP concern their excessively high Néel temperature that we can roughly estimate to  $\sim 700 \text{ K}$  from the amplitude of the ordered moments at RT,

in agreement with the moment reduction expected for  $S = 5/2$  Brillouin curve when  $T/T_{\text{N}} \approx 0.4$ . The same extrapolation can be performed on several high  $T_{\text{N}}$  oxides such as Sr<sub>2</sub>Fe<sub>2</sub>O<sub>5</sub>,<sup>33</sup> Ca<sub>2</sub>Fe<sub>2</sub>O<sub>5</sub>,<sup>34</sup> LaCa<sub>2</sub>Fe<sub>3</sub>O<sub>8</sub>, and Ba<sub>1.6</sub>Ca<sub>2.3</sub>Y<sub>1.1</sub>Fe<sub>5</sub>O<sub>13</sub><sup>35</sup> that also show  $M(\text{Fe}^{3+}) \approx 3.5 \mu_{\text{B}}$  at RT and  $T_{\text{N}} > 700 \text{ K}$ . In these oxides, the high  $T_{\text{N}}$  arises from strong  $\sim 180^\circ$  Fe<sup>3+</sup>–O–Fe<sup>3+</sup> super-exchanges. In both FHP, it comes out that  $T_{\text{N}} \approx 700 \text{ K}$  corresponds to the most robust antiferromagnetism observed in the broad series of hexagonal-perovskite. For comparison, it is worth recalling that in the nonfluorinated 6H-BaFeO<sub>3- $\delta$</sub> ,  $T_{\text{N}}$  is below 130 K.<sup>36</sup> As detailed above (Figure 3), we have not been able to prepare the 6H-BaFeO<sub>3- $\delta$</sub>  oxide with predominant Fe<sup>3+</sup>, with a significant contribution of tetrahedral dimers, and the magnetism of our nonfluorinated sample looks similar to reported characterizations. For the 15R-FHP, the comparison is less relevant because oxides were only prepared with a significant amount of Ir<sup>4+</sup>/Mn<sup>4+</sup> in the B site ( $M = \text{Ir}^{4+}, \text{Mn}^{4+}$ ) and all show  $T_{\text{N}}$  lower than 220 K. In FHPs, the persistence of the magnetic ordering until high temperature has been probed by both high-temperature magnetization measurements and Mössbauer spectroscopy.

We examined carefully these data, taking into account the complex redox chemistry of FHP mentioned above. In fact, in situ XRD show that their ability to incorporate/remove oxygen on heating/cooling through anion rearrangement corresponds to a reversible oxidation of Fe<sub>2</sub>O<sub>7</sub> pairs into Fe<sub>2</sub>O<sub>9- $x$</sub>  pairs, while O, F, and vacancies reorganize within the h-layers.<sup>13</sup> Therefore, thermal magnetization measurements in air and flowing N<sub>2</sub> diverge below  $T_{\text{N}}$ , reminiscent of the redox changes. We find  $T_{\text{N}} = 680 \text{ K}$ ,  $\theta_{\text{Cw}} = -470 \text{ K}$ ,  $\mu_{\text{eff}} = 4.42 \mu_{\text{B}}/\text{Fe}$  for the 15R-BaFeF<sub>0.2</sub>O<sub>3- $y$</sub>  and  $T_{\text{N}} = 710 \text{ K}$ ,  $\theta_{\text{Cw}} = -1357 \text{ K}$ ,  $\mu_{\text{eff}} = 5.25 \mu_{\text{B}}/\text{Fe}$  for the 6H-FHP Ba<sub>0.8</sub>Sr<sub>0.2</sub>FeF<sub>0.2</sub>O<sub>3- $y$</sub> , from the data collected under N<sub>2</sub> upon

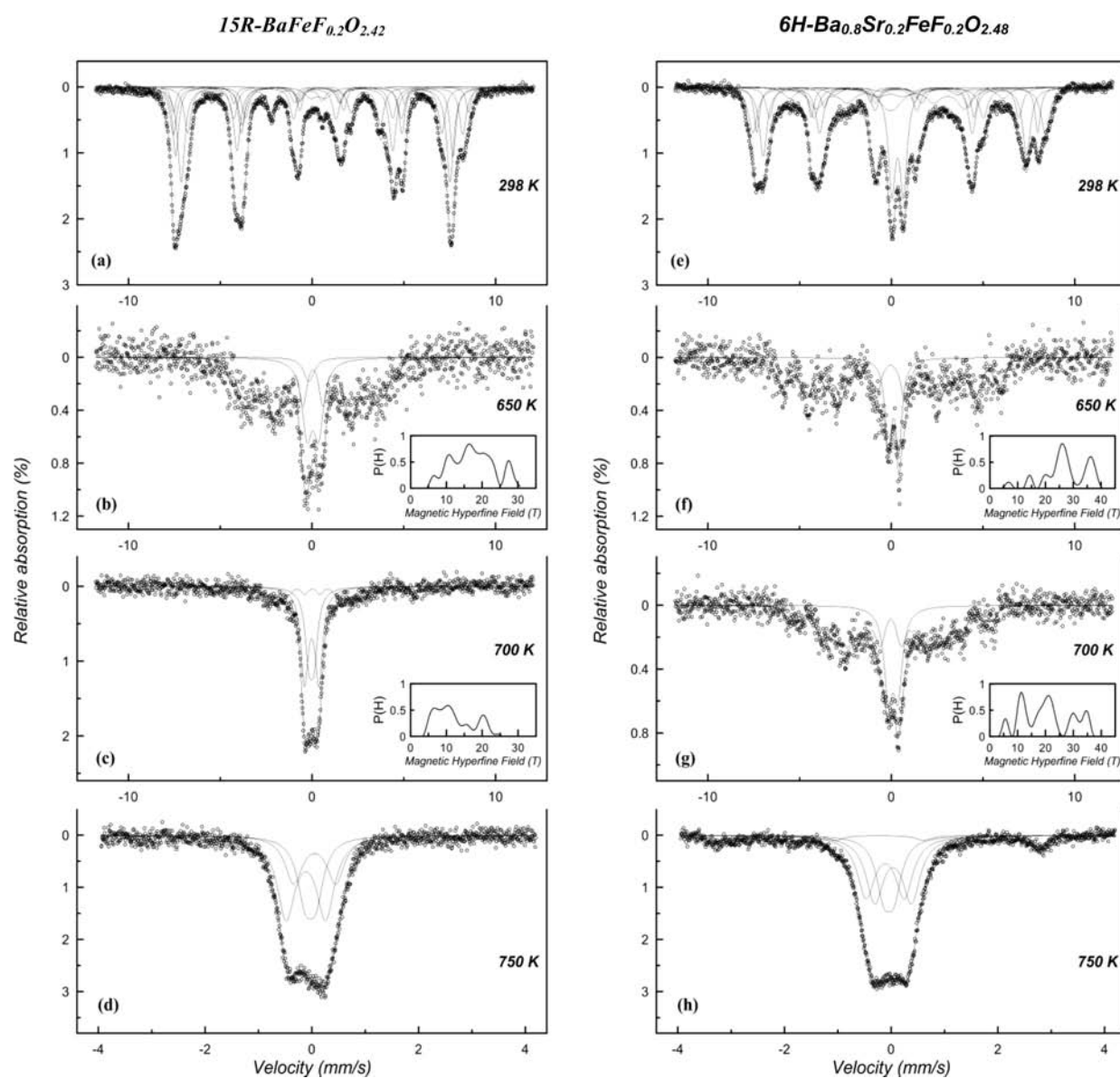


**Figure 4.**  $^{57}\text{Fe}$  Mossbauer spectra of (a–d) 15R- and (e–h) 6H-FHP recorded in Ar at temperatures indicated (insets show the corresponding magnetic field distributions).

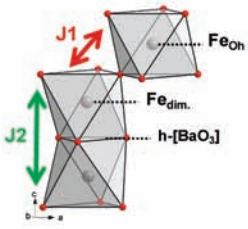
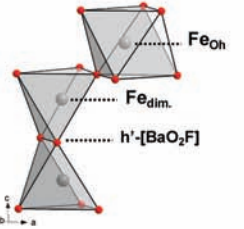
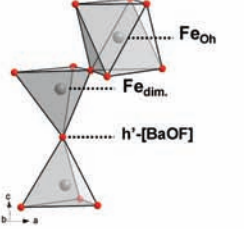
heating Figure 2e,f. The high magnitudes of  $\theta_{\text{Cw}}$  comfort the strong dominant AFM exchanges in both compounds. The  $\mu_{\text{eff}}$  values are in good agreement with the majority of  $\text{Fe}^{3+}$  deduced from PND and redox titration ( $\mu_{\text{eff}} = 5.91 \mu\text{B}/\text{Fe}$  in the spin-only model).

Magnetization curves also show that below  $T_{\text{N}}$ , antiferromagnetism is accompanied by a weak remanent moment of 0.03 and 0.01  $\mu\text{B}/\text{f.u.}$  at room temperature for the 15R and 6H tested compounds (Supporting Information S4). It likely results from the presence in the hexagonal slabs of various iron coordinations and valence states, although the  $\text{Fe}^{3+}$  predominates. It should generate competition between antagonist exchanges, such as AFM  $\text{Fe}^{3+}-\text{O}-\text{Fe}^{3+}$  but also less numerous FM  $\text{Fe}^{4+}-\text{O}-\text{Fe}^{4+}$  superexchanges. This disorder could result in uncompensated AFM alignment or FM local aggregate. This behavior, which combines AFM and weak FM, is reminiscent of what is observed for the 6H-BaFeO $_{3-\delta}$  oxide in which magnetic domains exist

below 170 K and cohabit with a long-range AFM ordering below  $T_{\text{N}} = 130 \text{ K}$ .<sup>36</sup> The randomly distributed frustrations were assigned to the competition of the magnetic interactions between Fe spins with different S in the local region. However, this analogy with our 6H-FHP is rather limited due to the persistence of AFM until 730 K.

**Mössbauer Spectroscopy.** For a clear vision of the “as-prepared” magnetic states, high-temperature Mössbauer spectroscopy was performed under both air and argon. For reasons of clarity, the results obtained under argon will be presented here, even though the partial reduction of the samples in this static gas cannot be fully avoided, as suggested for the 6H compound by TGA in more reducing conditions (flowing Ar). The ambient temperature Mössbauer spectra of both the 15R and the 6H compounds are shown in Figure 4. The spectra are magnetically split, and each of them mainly consists of overlapped broadened Zeeman sextets (Table 1). The isomer shifts (IS) for the major components ranged between 0.19 and 0.38 mm/s

Table 2. Local Structure of the Optimized Structural Models 6H-BaFeO<sub>3</sub>, 6H-BaFeO<sub>2.66</sub>F<sub>0.33</sub>, and 6H-BaFeO<sub>2.33</sub>F<sub>0.33</sub>, and the Corresponding *J* Values (*J*<sub>1</sub> and *J*<sub>2</sub>) Together with the Calculated Magnetic Moments Obtained from the AF1 Magnetic Configuration (See Figure S1d)

| Compound                                       |                          | 6H-BaFeO <sub>3</sub> (Fe <sup>4+</sup> )   | 6H-BaFeO <sub>2.66</sub> F <sub>0.33</sub> (Fe <sup>3.66+</sup> )                  | 6H-BaFeO <sub>2.33</sub> F <sub>0.33</sub> (Fe <sup>3+</sup> )                      |
|--|--------------------------|---|--|---|
| <b>Local Environment</b>                       |                          |  |  |  |
| J1   | d <sub>(Fe-Fe)</sub> (Å) | 3.873   | 3.82-3.92  | 3.822/3.792   |
|  | <Fe-O-Fe                 | 177.21°   | 170.1°-175.7°  | 165.2°/164.3°   |
|  | J1 (K)                   | 123.21  | -5.90  | -115.04   |
| J2   | d <sub>(Fe-Fe)</sub> (Å) | 2.572   | 2.758  | 3.476   |
|  | <Fe-O-Fe                 | 85.62°  | 94.9°-95.0°  | 171.07°   |
|  | J2 (K)                   | -41.17  | -79.54   | -247.26   |
| <i>DFT calculated Fe atoms magnetic moment</i> |                          |   |  |   |
| M(Fe <sub>Oh</sub> ) (μB)                      |                          | 3.48  | 4.19   | 4.04  |
| M(Fe <sub>dim.</sub> ) (μB)                    |                          | 4.19  | 3.59   | 4.18  |

corresponding to the high spin Fe<sup>3+</sup>. The sextets with highest IS's and highest values of magnetic hyperfine fields, *H*<sub>hf</sub>'s, that is, A1, A2 and C1 for 15R- and 6H-FHP, respectively, are to be attributed to the octahedrally coordinated sites. The sextets A3, A4, A5 (in 15R) and C2, C3, C4 (in 6H) could be assigned to the Fe<sup>3+</sup> cations in Fe<sub>2</sub>(O,F)<sub>9-x</sub> dimers around h-layers: A3, A4 and C2, C3 in Fe<sub>2</sub>O<sub>6</sub>(O,F)<sub>2</sub> pyramidal pairs and A5 and C4 in Fe<sub>2</sub>O<sub>7</sub> tetrahedral pairs. The observed IS's values for these sextets are typical for Fe<sup>3+</sup> cations in oxides and somewhat lower than those reported for oxo-fluorides with high degrees of fluorination, for example, BaFeO<sub>2</sub>F.<sup>37,38</sup> This suggests that F<sup>-</sup> anions do not directly involve in the Fe coordination and thus backs up the structural models. The correlation between the relative contributions of sextets with results from NPD is rather difficult considering the presence of Fe<sup>4+</sup> cations likely distributed on several crystallographic positions, Table 1. Indeed, low IS's Fe<sup>4+</sup> components are mostly magnetically split (A6, A7 and C7, C8 in Table 1) and, especially for the 6H FHP, substantially broadened. The deduced Fe mean valence from the Mössbauer Fe<sup>4+</sup> partial contributions (Fe<sup>+3.15</sup> and Fe<sup>+3.19</sup> for the 15R and the 6H compounds, respectively) is in rather good agreement with chemical titration and NPD. Besides, there are two additional broadened Fe<sup>3+</sup> components in the 6H spectrum (sextet C5, paramagnetic C6), which are likely a result of spin relaxation of

Fe<sup>3+</sup> caused by a combination of several factors, particles size distribution, mixed Fe<sup>3+</sup>/Fe<sup>4+</sup> valence, and structural defects.

High-temperature Mössbauer spectra in static Ar confirm the transition of both FHPs at elevated temperature. It is notable that this transition is extended over the wide temperature range of about 150 K, where magnetic and paramagnetic spectral components coexist, which is reminiscent of defected magnetic structures. The magnetic components completely vanished from the spectra at temperatures close to 750 K that correlates well with the *T*<sub>N</sub> values of about 700–730 K for both compounds as determined by magnetic susceptibility measurements (Figure 4). The spectra at 750 K can be described by a superposition of several unresolved paramagnetic doublets. In the 6H spectrum, the minor magnetically split D4 component presumably belongs to an impurity with higher *T*<sub>N</sub>, which could result from the partial reduction on heating in Ar. Despite strong overlapping of doublets, the robust fitting of the 15R and 6H spectra was achieved with three doublets, as shown in Figure 4d,h, with parameters agreeing excellently with the ambient temperature values. According to their hyperfine parameters, doublets B1 and D1 are to be attributed to the octahedral positions, while B2/D2 and B3/D3 are attributed to 5-fold and tetrahedrally coordinated sites around h-layers, respectively. It is worth mentioning that IS's of all of the

doublets correspond, with respect to the second-order Doppler temperature shift,<sup>38</sup> to Fe<sup>3+</sup>, and thus lack of the Fe<sup>4+</sup> components is observed, which comforts the partial reduction of those compounds under current conditions and the absence of octahedral pairs bordering the h-layers.

**Theoretical Certification.** To assign the physical origin of the abnormally robust antiferromagnetism of Fe-FHP, we examined the magnetic properties of the 6H-BaFeO<sub>3</sub> and fluorinated derivatives from the viewpoint of two super exchange paths,  $J_1$  and  $J_2$  (Table 2), through first-principles density functional theory (DFT) calculations. We consider different structural models by introduction of F<sup>-</sup> into the ideal oxide 6H-BaFeO<sub>3</sub> (Figure S1b). h<sup>-</sup>[BaOF] layers lead to corner-sharing tetrahedra, while h<sup>-</sup>[BaO<sub>2</sub>F] layers yield edge-sharing pyramids (Table 2 and Figure S1b). All structures were fully relaxed using the VASP program (Supporting Information S1). Distances and angles of interest are reported in Table 2 as well as the magnetic exchange coupling ( $J_1$  and  $J_2$ ) and the calculated magnetic moments on the iron atoms, Fe<sub>dim</sub> and Fe<sub>oh</sub>. To access  $J_1$  and  $J_2$  values, the total energies of three ordered spin states were calculated (Supporting Information S1). The strong electronic correlation associated with the Fe 3d states was taken into account using GGA+U calculations with  $U_{\text{eff}} = 5$  eV. This value was taken from the literature dealing with the related BaFeO<sub>3</sub>,<sup>39</sup> in addition,  $U_{\text{eff}}$  values in the range 4–6 eV lead to qualitatively the same results. The energies of these ordered spin states are expressed using the spin Hamiltonian  $\hat{H} = -\sum_{i<j} J_{ij} \hat{S}_i \cdot \hat{S}_j$ , where  $J_{ij} = (J_1, J_2)$  corresponds to the exchange between spins  $i$  and  $j$ .  $J_1$  and  $J_2$  are then extracted according to the procedure detailed in the Supporting Information.

For the 6H-BaFeO<sub>3</sub>, we found  $|J_{1(\text{FM})}| > |J_{2(\text{AFM})}|$ , consistent with 180° and 90° Fe<sup>4+</sup>–O–Fe<sup>4+</sup> superexchanges (Fe–O–Fe = 177.2° and 85.6° from the Kanamori–Goodenough rules).<sup>40</sup> The passage from octahedral to tetrahedral pairs (via pyramidal dimers) is accompanied by a reversal of  $J_1$  sign from FM to AFM, while  $J_{2(\text{AFM})}$  becomes strongly predominant. In the 6H-BaFeO<sub>2.33</sub>F<sub>0.33</sub> end-member compound, the AFM interactions are consistent with the predicted 180° Fe<sup>3+</sup>–O–Fe<sup>3+</sup> exchanges (Fe<sub>dim</sub>–O–Fe<sub>dim</sub> = 171.07° and Fe<sub>dim</sub>–O–Fe<sub>oh</sub> = 165.16°). Therefore, the changes in Fe–O–Fe connectivity after fluorine insertion in h-layers drive drastic increases of  $J_2$  exchanges, while they approach 180° superexchanges. It is difficult to separate the effects of the geometrical changes and of the Fe<sup>4+</sup> ( $S = 2$ ) to Fe<sup>3+</sup> ( $S = 5/2$ ) reduction. The geometrical effect could be more involved in the  $J_2$  changes, at the origin of robust intratetrahedral AFM. The valence effect should mostly influence  $J_1$ , responsible for the FM → ~0 → AFM transition, while the Fe–O–Fe angle smoothly varies from 177° to 165°.

The calculated spin moment values given in Table 2 are consistent with high spin states in all sites for the three structures, as experimentally observed in the disordered 6H and 15R forms. However, these values should not be taken too literally, due to the calculation method and to covalent diluting effects.

It is striking that according to PND and Mössbauer results for both the 6H and the 15R archetypes, hexagonal interleaves consist of about 30% of tetrahedral dimers, while the remaining part mostly have 5-fold configurations. So, the high  $T_N \approx 700$  K reflects the impact of a minority of the tetrahedral dimers on the collective magnetic ordering. It is such that FHP magnetically order well above other iron hexagonal perovskites ( $T_N = 172$  K in 12H-BaFeO<sub>3- $\delta$</sub> ,<sup>41</sup>  $T_N = 130$  K in 6H-BaFeO<sub>3- $\delta$</sub> ,<sup>36</sup>  $T_N < 220$  K in Ba(Fe,M)O<sub>3- $\delta$</sub> )<sup>22,23</sup> and reach values of corner-sharing Fe oxides derived from the cubic perovskite ( $T_N = 740$  K in LaFeO<sub>3</sub>)<sup>42</sup> and

hexa-ferrite materials ( $T_C$  for BaFe<sub>12</sub>O<sub>19</sub> = 726 K).<sup>43</sup> A most exhaustive list of concerned compounds is given in the Supporting Information S5.

## CONCLUSION

The possibility to tune magnetic/electric properties playing on the anionic sublattice is offered by the insertion of fluorine. A number of examples exist in which mixed O<sup>2-</sup>/F<sup>-</sup> or interstitial F<sup>-</sup> accommodate metal redox changes responsible for spectacular modifications of the properties, that is, ferromagnetic Sr<sub>2</sub>Mn<sub>2</sub>(O,F)<sub>6</sub>,<sup>44</sup> superconducting Sr<sub>2</sub>CuO<sub>2</sub>F<sub>2+ $\delta$</sub> ,<sup>45</sup> or AFM-BaCoF<sub>x</sub>O<sub>3- $y$</sub> ,<sup>25,27,30</sup> polytypes issued from FM-BaCoO<sub>3- $\delta$</sub> ,<sup>46,47</sup> polytypes. We have demonstrated in iron FHP that the concomitant effects of the Fe<sup>4+</sup> to Fe<sup>3+</sup> reduction and the subsequent modifications of a part of the Fe–O–Fe connectivity influence the collective magnetic ordering toward highest  $T_N$  (~700 K) observed in the broad family of hexagonal perovskites. The incorporation of fluorine in the hexagonal network is accompanied by the replacement of face-sharing by edge/corner-sharing dimers, while in practice leading to an extended defect structure that combines all topologies. Our DFT calculations confirm that the Fe–Fe magnetic exchanges involved in the hexagonal interleave gradually increase along the Fe<sub>2</sub>O<sub>9</sub> → Fe<sub>2</sub>O<sub>8</sub> → Fe<sub>2</sub>O<sub>7</sub> transformation, responsible for the unprecedented robust AFM within diversified topologies.

## ASSOCIATED CONTENT

**S Supporting Information.** Details of ab initio calculations, neutron diffraction (ND), and magnetic measurements for several 15R-FHP and 6H-FHP samples; additional figures as noted in the text. This material is available free of charge via the Internet at <http://pubs.acs.org>.

## AUTHOR INFORMATION

**Corresponding Author**  
olivier.mentre@ensc-lille.fr

## ACKNOWLEDGMENT

We are grateful to Laboratoire Leon Brillouin (LLB, Saclay, France) for PND measurements. The “Fonds Européens de Développement Régional (FEDER)”, CNRS, “Région Nord Pas-de-Calais”, and “Ministère de l’Éducation Nationale de l’Enseignement Supérieur et de la Recherche” are acknowledged for fundings of X-ray diffractometers. The “Agence Nationale pour la Recherche” is thanked for financial support through the MAD-BLAST project ref ANR-09-BLAN-0187-01. We thank the USTL Centre de ressources informatiques (partially funded by FEDER) for allocating CPU time. This work was carried out under the framework of the MAD-BLAST project supported by the ANR (grant No. ANR-09-BLAN-0187-01).

## REFERENCES

- (1) Wolf, S. A.; Awschalom, D. D.; Buhrman, R. A.; Daughton, J. M.; Molnár, S.; Roukes, M. L.; Chtchelkanova, A. Y.; Treger, D. M. *Science* **2001**, *294*, 1488–1495.
- (2) Xiu, F.; Wang, Y.; Kim, J.; Hong, A.; Tang, J.; Jacob, A. P.; Zou, J.; Wang, K. L. *Nat. Mater.* **2010**, *9*, 337–344.
- (3) Parkin, S. S. P.; Kaiser, C.; Panchula, A.; Rice, P. M.; Hughes, B.; Samant, M.; Yang, S. H. *Nat. Mater.* **2004**, *3*, 862–867.



- (4) Nogués, J.; Schuller, I. K. *J. Magn. Magn. Mater.* **1999**, *192*, 203–232.
- (5) Nowak, U.; Usadel, K. D.; Keller, J.; Miltényi, P.; Beschoten, B.; Guntherodt, G. *Phys. Rev. B* **2002**, *66*, 14430.
- (6) Chen, W.; Williams, A. J.; San-Martin, L. O.; Li, M.; Sinclair, D. C.; Zhou, W.; Atfield, J. P. *Chem. Mater.* **2009**, *21*, 2085–2093.
- (7) Sievers, A. J.; TinKham, M. *Phys. Rev.* **1963**, *129*, 1566–1571.
- (8) Nagamiya, T.; Saito, S.; Shimomura, Y.; Uchida, E. *J. Phys. Soc. Jpn.* **1965**, *20*, 1285–1286.
- (9) Lebeugle, D.; Colson, D.; Forget, A.; Viret, M.; Bataille, A. M.; Gukasov, A. *Phys. Rev. Lett.* **2008**, *100*, 227602.
- (10) Tsujimoto, Y.; Tassel, C.; Hayashi, N.; Watanabe, T.; Kageyama, H.; Yoshimura, K.; Takano, M.; Ceretti, M.; Ritter, C.; Paulus, W. *Nature* **2007**, *450*, 1062–1065.
- (11) Pruneda, J. M.; Íñiguez, J.; Canadell, E.; Kageyama, H.; Takano, M. *Phys. Rev. B* **2008**, *78*, 115101.
- (12) Xiang, H. J.; Wei, S.-H.; Whangbo, M.-H. *Phys. Rev. Lett.* **2008**, *100*, 167207.
- (13) Sturza, M.; Daviero-Minaud, S.; Kabbour, H.; Gardoll, O.; Mentré, O. *Chem. Mater.* **2010**, *22*, 6726–6735.
- (14) Mori, K.; Kamiyama, T.; Kobayashi, H.; Oikawa, K.; Otomo, T.; Ikeda, S. *Phys. Soc. Jpn.* **2003**, *72*, 2024–2028.
- (15) Carvajal, R. *J. Physica B* **1993**, *55*, 192 (program Fullprof available from <http://www-llb.cea.fr/fullweb/fp2k/fp2k.htm>).
- (16) Kresse, G.; Furthmüller, J. *Vienna Ab-initio Simulation Package (VASP)*; Institut für Materialphysik: Vienna, 2004; <http://cms.mpi.univie.ac.at/vasp>.
- (17) Kresse, G.; Joubert, D. *Phys. Rev. B* **1999**, *59*, 1758.
- (18) Perdew, J. P.; Wang, Y. *Phys. Rev. B* **1992**, *45*, 13244.
- (19) Dudarev, S. L.; Botton, G. A.; Savrasov, S. Y.; Humphreys, C. J.; Sutton, A. P. *Phys. Rev. B* **1998**, *57*, 1505.
- (20) Adkin, J. J.; Hayward, M. A. *Chem. Mater.* **2007**, *19*, 755–762.
- (21) Kuo, J. H.; Anderson, H. U.; Sparlin, D. M. *J. Solid State Chem.* **1989**, *83*, 52–60.
- (22) Jordan, N. A.; Battle, P. D.; Sloan, J.; Manuel, P.; Kilcoyne, S. *J. Mater. Chem.* **2003**, *13*, 2617–2625.
- (23) Cussen, E. J.; Sloan, J.; Vente; Battle, P. D.; Gibb, T. C. *Inorg. Chem.* **1998**, *37*, 6071–6077.
- (24) Yamaura, K.; Young, D. P.; Siegrist, T.; Besnard, C.; Svensson, C.; Liu, Y.; Cava, R. J. *J. Solid State Chem.* **2001**, *158*, 175–179.
- (25) Ehora, G.; Renard, C.; Daviero-Minaud, S.; Mentré, O. *Chem. Mater.* **2007**, *19*, 2924–2926.
- (26) Tancret, N.; Roussel, P.; Abraham, F. *J. Solid State Chem.* **2005**, *178*, 3066–3073.
- (27) Mentré, O.; Kauffmann, M.; Ehora, G.; Daviero-Minaud, S.; Abraham, F.; Roussel, P. *J. Solid State Sci.* **2008**, *10*, 471–475.
- (28) Kauffmann, M.; Mentré, O.; Legris, A.; Hébert, S.; Pautrat, A.; Roussel, P. *Chem. Mater.* **2008**, *20*, 1741–1749.
- (29) Kauffmann, M.; Mentré, O.; Legris, A.; Tancret, N.; Abraham, F.; Roussel, P. *Chem. Phys. Lett.* **2006**, *432*, 88–93.
- (30) Mentre, O.; Kabbour, H.; Ehora, G.; Tricot, G.; Daviero-Minaud, S.; Whangbo, M. H. *J. Am. Chem. Soc.* **2010**, *132*, 4865–4875.
- (31) Clements, O.; Haberkorn, R.; Slater, P. R.; Beck, H. P. *J. Solid State Sci.* **2010**, *12*, 1455–1463.
- (32) Ivanova, S. A.; Eriksson, S.-G.; Erikssenc, J.; Tellgrend, R.; Rundlofd, H. *Mater. Res. Bull.* **2004**, *39*, 615–628.
- (33) Schmidt, M.; Campbell, S. J. *J. Solid State Chem.* **2001**, *156*, 292–304.
- (34) Berastegui, P.; Eriksson, S.-G.; Hull, S. *Mater. Res. Bull.* **1999**, *34*, 303–314.
- (35) Demont, A.; Dyer, M. S.; Sayers, R.; Thomas, M. F.; Tsiamtsouri, M.; Niu, H. N.; Darling, G. R.; Daoud-Aladine, A.; Claridge, J. B.; Rosseinsky, M. J. *Chem. Mater.* **2010**, *22*, 6598–6615.
- (36) Mori, K.; Kamiyama, T.; Kobayashi, H.; Otomo, T.; Nishiyama, K.; Sugiyama, M.; Itoh, K.; Fukunaga, T.; Ikeda, S. *J. Appl. Crystallogr.* **2007**, *40*, 501–505.
- (37) Heap, R.; Slater, P. R.; Berry, F. J.; Helgason, O.; Wright, A. J. *Solid State Commun.* **2007**, *141*, 467–470.
- (38) Menil, F. *J. Phys. Chem. Solids* **1985**, *46*, 763–789.
- (39) Hong-Jian, F.; Fa-Min, L. *Chin. Phys. B* **2008**, *17*, 187–1880.
- (40) Goodenough, J. B. *Magnetism and the Chemical* Wiley-Interscience: New York, 1963.
- (41) Takeda, Y.; Shimada, M.; Kanamaru, F.; Koizumi, M.; Yamamoto, N. *Mater. Res. Bull.* **1974**, *4*, 537–543.
- (42) Seo, J. W.; Fullerton, E. E.; Nolting, F.; Scholl, A.; Fompeyrine, J.; Locquet, J.-P. *J. Phys.: Condens. Matter* **2008**, *20*, 264014.
- (43) Wang, J.; Chen, Q.; Chea, S. *J. Magn. Magn. Mater.* **2004**, *280*, 281–286.
- (44) Lobanov, M. V.; Abakumov, A. M.; Sidorova, A. V.; Rozova, M. G.; D'yachenko, O. G.; Antipov, E. V.; Hadermann, J.; Tendeloo, G. V. *J. Solid State Sci.* **2002**, *4*, 19–22.
- (45) Al-Mamouri, M.; Edwards, P. P.; Greaves, C.; Slaski, M. *Nature* **1994**, *369*, 382–384.
- (46) Pardo, V.; Blaha, P.; Iglesias, M.; Schwarz, K.; Baldomir, D.; Arias, J. E. *Phys. Rev. B* **2004**, *70*, 144422.
- (47) Yamaura, K.; Cava, R. J. *Solid State Commun.* **2000**, *115*, 301.